Heat Capacity of a Strongly-Interacting Fermi Gas: Supporting Online Material

J. Kinast,[1] A. Turlapov,[1] J. E. Thomas,[1*]
Qijin Chen,[2] Jelena Stajic,[2] and K. Levin[2]

[1]Physics Department, Duke University, Durham, North Carolina 27708-0305, USA
[2]James Franck Institute and Department of Physics, University of Chicago,
5640 South Ellis Avenue, Chicago, Illinois 60637, USA

[*]To whom correspondence should be addressed; E-mail: jet@phy.duke.edu.

Materials and Methods

Computation of Thermodynamical Quantities

The theoretical community is in the midst of unraveling the nature of resonantly interacting fermionic superfluids (*S1–S9*) with particular emphasis on the strongly interacting Fermi gas (*S10*). In the BCS-BEC crossover picture (*S11*), the strongly interacting Fermi gas is intermediate between the weak coupling BCS and BEC limits. In addressing the nature of the excitations from the conventional mean field or BCS-like ground state (*S12*), our theoretical calculations help to provide a theoretical calibration of the experimental thermometry, and elucidate the thermodynamics.

Without doing any calculations one can anticipate a number of features of thermodynamics in the crossover scenario. The excitations are entirely bosonic in the BEC regime, exclu-

sively fermionic in the BCS regime, and in between both types of excitation are present. In the so-called one-channel problem the "bosons" correspond to noncondensed Cooper pairs, whereas in two-channel models, these Cooper pairs are strongly hybridized with the molecular bosons of the closed channel, singlet state. Below T_c the presence of the condensate leads to a single-branch bosonic excitation spectrum which, at intermediate coupling, is predominantly composed of large Cooper pairs. These latter bosons lead to a pseudogap (*S11, S13*) above T_c. Within the conventional mean field ground state, and over the entire crossover regime (*S14*) below T_c, the bosons with effective mass M^* have dispersion $\Omega_q = \hbar^2 q^2/2M^*$. This form for the dispersion reflects the absence of direct boson-boson interactions. In the extreme BEC limit, when the fermionic degrees of freedom become irrelevant, direct inter-boson interactions must be accounted for. While our focus in this paper is on the unitary case, when we refer to "BEC" we restrict our attention to the near-unitary BEC regime.

As long as the attractive interactions are stronger than those of the BCS regime, these non-condensed pairs must show up in thermodynamics, as must the pseudogap in the fermionic spectrum. These are two sides of the same coin. Below T_c, the fermionic excitations have dispersion $E_{\mathbf{k}} = \sqrt{(\epsilon_{\mathbf{k}} - \mu)^2 + \Delta^2}$, where $\epsilon_{\mathbf{k}} = \hbar^2 k^2/2m$ and μ are the atomic kinetic energy and fermionic chemical potential, respectively. That this excitation gap Δ is non-zero at T_c in the Bogoliubov quasi-particle spectrum $E_{\mathbf{k}}$, differentiates the present approach (*S14*) from all other schemes which address BCS-BEC crossover at finite T. The bosons, by contrast, are gapless in the superfluid phase, due to their vanishing chemical potential. Within a trap, and in the fermionic regime (for which $\mu > 0$), the fermionic component will have a strong spatial inhomogeneity via the spatial variation of the gap. Thus, in contrast to the homogeneous case, fermions on the edge of the trap, which have relatively small or vanishing excitation gaps Δ, will contribute power law dependences to the thermodynamics.

Starting at a magnetic field well above a Feshbach resonance, by decreasing the magnetic

field, we tune from the BCS-like regime towards unitarity at resonance. We first consider low T where fermions become paired over much of the trap. The unpaired fermions at the edge tend to dominate the thermodynamics associated with the fermionic degrees of freedom, and lead to a higher (than linear) power law in the T dependence of the entropy. The contribution from excited pairs of fermions is associated with a $T^{3/2}$ dependence of entropy on temperature which dominates for temperatures $T/T_F \lesssim 0.05$ or $T/T_c \lesssim 0.2$. In general, the overall exponent of the low T power law varies with magnetic field, depending on the magnitude of the gap and temperature, as well as the relative weight of fermionic and bosonic contributions. In the superfluid phase, at all but the lowest temperatures, the fermions and bosons combine to yield $S \propto T^2$ precisely at resonance ($(k_F a)^{-1} = 0$). For the near-unitary case investigated in the paper ($(k_F a)^{-1} = 0.11$), we have $S \propto T^{1.9}$.

Because our calculations (*S15*) are based on the standard mean field ground state (*S12*), we differ from other work (*S2, S16*) at finite temperatures. Elsewhere (*S13, S14, S17*) we have characterized in quantitative detail the characteristic gap Δ and pseudogap Δ_{pg} energy scales. The pseudogap (which is to be associated with a hybridized mix of noncondensed fermion pairs and molecular bosons) and the superfluid condensate (sc) called $\tilde{\Delta}_{sc}$, add in quadrature to determine the fermionic excitation spectrum: $\Delta^2(T) = \tilde{\Delta}^2_{sc}(T) + \Delta^2_{pg}(T)$. Our past work (*S13, S14, S17*) has primarily focussed below T_c. Here we extend these results, albeit approximately, above T_c. Our formalism has been applied below T_c with some success in Ref. (*S8*) to measurements of the pairing gap in RF spectroscopy. A more precise, but numerically more complex method for addressing the normal state was given in Ref. (*S18*).

After including the trap potential $U(r)$ and internal binding energy of the bosons, the local energy density can be decomposed into fermionic (E_f) and bosonic (E_b) contributions and

directly computed as follows

$$\begin{aligned} E &= \mu n(r) + E_f + E_b \,, \\ E_f &= \sum_K (i\omega_n + \epsilon_{\mathbf{k}} - \mu(r)) G(K) \\ &= \sum_{\mathbf{k}} [2E_{\mathbf{k}} f(E_{\mathbf{k}}) - (E_{\mathbf{k}} - \epsilon_{\mathbf{k}} + \mu(r))] + \Delta^2 \chi(0) \,, \\ E_b &= \sum_q (\Omega_{\mathbf{q}} - \mu_{boson})\, b(\Omega_{\mathbf{q}} - \mu_{boson}) \,, \end{aligned} \tag{S1}$$

where $\mu(r) = \mu - U(r)$, $n(r)$ is the local density, $\omega_n = (2n+1)\pi k_B T$ is the fermionic Matsubara frequency, $G(K)$ is the renormalized fermionic Green's function with four-momentum $K \equiv (i\omega_n, \mathbf{k})$, $b(x)$ and $f(x)$ are the Bose and Fermi distribution functions, respectively. The pair susceptibility $\chi(0)$, at zero frequency and zero momentum, is given by

$$\chi(0) = \sum_{\mathbf{k}} \frac{1 - 2f(E_{\mathbf{k}})}{2E_{\mathbf{k}}} \tag{S2}$$

and the bosonic chemical potential μ_{boson} is zero in the superfluid phase.

Unlike the situation in condensed matter systems, for these ultracold gases, thermometry is less straightforward. Experimentally, temperature is determined from the spatial profiles of the cold gas, either in the trap, or following expansion. For weakly interacting Bose and Fermi gases, where the theoretical density is well understood, this procedure is straightforward. However, for a strongly interacting gas, the spatial profile has not been understood until recently (*S17*). For this reason, the temperature is often measured on either side far away from the Feshbach resonance, where the scattering length is small. A strongly interacting sample in the unitary regime is then prepared by an adiabatic change of the magnetic field.

More specifically, in the BCS or weak attraction regime, temperature is determined by fitting the spatial (or momentum distribution) profiles to those of a non-interacting Fermi gas (*S19*). In the opposite BEC regime, temperature can be deduced by fitting the Gaussian wings of density profiles or determining condensate fractions (*S20*, *S21*). Thus, it is convenient to describe a

given intermediate regime which is accessed adiabatically, by giving the initial temperature at either endpoint. In order to determine this adiabatically accessed temperature, one needs precise knowledge of the entropy S as a function of T and magnetic field from BCS to BEC. The entropy S can be calculated directly (*S15*) as a sum of fermionic and bosonic contributions based on the two types of excitations. Equivalently, one can also calculate the entropy from the energy, $S = \int_0^T \frac{dT}{T}\frac{dE}{dT}$.

In the strongly interacting regime, one can measure an empirical temperature $\tilde{T}$ by fitting a T-F density profile directly to the spatial distribution, as done in this paper. In the following, we describe a temperature calibration method which relates the measured empirical temperature $\tilde{T}$ to the theoretical value of T/T_F.

Calibration of Experimental Temperature Scale

In order to obtain a temperature calibration curve for the experiments (inset, Fig. 2 main text) we note that our theoretically generated profiles yield very good agreement with the Thomas-Fermi functional form (*S17*) for the normal and superfluid states. However, there are slight systematic deviations from this form in the superfluid phase. Below T_c the profiles contain the superfluid condensate as well as non-condensed pairs along with excited fermions. Although our profiles are generated for an isotropic trap, it can easily be shown that trap anisotropy is not relevant for thermodynamic quantities. Because they involve integrals over the entire trap, the calculations can be mapped onto an equivalent isotropic system.

Our theoretical profiles are generated for given reduced temperatures T/T_F. If one applies the experimental procedure to these theoretical profiles one can deduce the parameter $\sqrt{1+\beta}\tilde{T}$ for each T/T_F. Theoretically, then, it is possible to relate these two temperature scales. This is summarized by the calibration curve in the inset to Figure 2.

Quite remarkably, it can be seen from this inset that the experimental T-F fitting procedure yields the precise theoretical temperature in the normal state. This applies even below the pseu-

dogap onset temperature T^*, since the non-condensed pairs and the fermions both are thermally distributed. However, in the superfluid phase, the parameter $\sqrt{1+\beta}\tilde{T}$ systematically underestimates the temperature, because of the presence of a condensate. One can understand this effect as arising principally from the fact that the region of the trap occupied by the condensate is at the center and decreases in radius as temperature is increased, until it vanishes at T_c. This prevents the profile from expanding with temperature as rapidly as for the non-interacting fermions of strict T-F theory. Hence, one infers an apparently lower temperature. As T/T_F approaches zero, the parameter $\sqrt{1+\beta}\tilde{T}$ must approach zero as well.

Experimental Methods and Empirical Thermometry

Preparation of the strongly interacting Fermi gas is described in the main text and the details can be found elsewhere (*S10, S22, S23*).

Preparation of degenerate, noninteracting Fermi gases follows a similar series of steps. As described previously (*S22*), 23 s of forced evaporation at 300 G brings the temperature of the gas to $\tilde{T} = 0.24$, the lowest temperature we can achieve in this case. The gas is then heated as described in the main text. Finally, the gas is released and imaged at 526 G to determine the number of atoms and the temperature. Temperatures $\tilde{T}$ between 0.24 and 1.23 are obtained for the noninteracting gas.

All heating and release for time of flight measurements are conducted at 4.6% of the full trap depth. At this depth, the measured trap frequencies, corrected for anharmonicity, are $\omega_\perp = \sqrt{\omega_x \omega_y} = 2\pi \times 1696(10)$ Hz and $\omega_z = 2\pi \times 72(5)$ Hz, so that $\bar{\omega} = (\omega_x \omega_y \omega_z)^{1/3} = 2\pi \times 592(14)$ Hz is the mean oscillation frequency.

For both the interacting and noninteracting samples, the column density is obtained by absorption imaging of the expanded cloud after 1 ms time of flight, using a two-level state-selective cycling transition (*S10, S22*). In the measurements, we take optical saturation into account exactly and arrange to have very small optical pumping out of the two-level system.

The resulting absorption image of the cloud can then be analyzed to determine the temperature of the sample.

Anharmonic Corrections to the Energy Input

Eq. 2 of the main text does not include corrections to the energy input which arise from anharmonicity in the gaussian beam trapping potential. In general, after the cloud expands for a time t_{heat}, the energy changes when the trapping potential $U(\mathbf{x})$ is abruptly restored,

$$\Delta E(t_{heat}) = \int d^3\mathbf{x}[n(\mathbf{x}, t_{heat}) - n_0(\mathbf{x})]U(\mathbf{x})\,. \tag{S3}$$

Here $n(\mathbf{x}, t_{heat})$ ($n_0(\mathbf{x})$) is the density of the expanded (trapped) cloud, where $n_0(\mathbf{x})$ is a zero temperature T-F profile, as noted in the main text. A scale transformation (*S24, S25*) relates $n(\mathbf{x}, t_{heat})$ to $n_0(\mathbf{x})$. Using this result, we obtain Eq. 2 of the main text as well as the anharmonic correction ΔE arising for a gaussian beam trapping potential. For a cylindrically symmetric trap, we obtain,

$$\frac{\Delta E}{E_0} = -\frac{\mu_0}{30\,U_0}\left[\,2b_\perp^4(t) + b_\perp^2(t) - 3\,\right] + \frac{\mu_0^2}{360\,U_0^2}\left[\,4b_\perp^6(t) + 2b_\perp^4(t) + 3b_\perp^2(t) - 9\,\right]. \tag{S4}$$

Note that for our experiments, we assume a gaussian beam potential with three different dimensions. These corrections are most significant for the largest values of t_{heat}, since the largest contribution to the energy change arises from atoms at the edges of the cloud.

Energy Input for Noninteracting Samples

Although the interacting and noninteracting samples are heated in the same fashion, there are a few differences in the way the energy input is calculated. In the noninteracting case, the correction factor in Eq. 2 of the main text, η_{nonint}, is determined at the lowest temperature $\tilde{T} = 0.24$ from the energy for an ideal Fermi gas. Furthermore, whereas the strongly interacting gas expands hydrodynamically, expansion of the noninteracting gas is ballistic so that $b_\perp(t_{heat}) = b_\perp^B(t_{heat}) = \sqrt{1 + (\omega_\perp t_{heat})^2}$.

Determination of β

We determine β by comparing the measured Fermi radius for the strongly interacting sample σ_x' to the calculated radius for a noninteracting gas σ_x confined in the same potential. The relation is given by $\sigma_x' = \sigma_x(1+\beta)^{1/4}$ (*S26*), where $\sigma_x = \sqrt{2k_B T_F/(M\omega_x^2)}$ is the radius for a noninteracting gas. We obtain $\sigma_x = 1.065\,(N/2)^{1/6}\,\mu$m for our trap parameters. This calculated radius is consistent with the value measured for noninteracting samples at 526 G in our trap. To determine σ_x', we measure the size of the cloud after 1 ms of expansion, and scale it down by the known hydrodynamic expansion factor of $b_\perp^H(1\,\text{ms}) = 13.3$ (*S10, S25*). We then determine the Fermi radius $\sigma_x' = 11.98\,(N/2)^{1/6}\,\mu\text{m}/13.3 = 0.901(0.021)\,(N/2)^{1/6}\mu$m. With these results, we obtain $\beta = -0.49(0.04)$ (statistical error only).

Observed Transition in Energy versus Empirical Temperature $\tilde{T}$

For the strongly interacting Fermi gas, without calibrating the empirical temperature scale, we observe a transition between two patterns of behavior at $\tilde{T} = 0.33$ (*S27*): For $\tilde{T} = 0.33 - 2.15$, we find that the energy closely corresponds to that of a trapped Fermi gas of noninteracting atoms with the mass scaled by $1/(1+\beta)$. At temperatures between $\tilde{T} = 0.04 - 0.33$, the energy scales as $\tilde{T}^{2.53}$, significantly deviating from ideal gas behavior as can be seen in Fig. S1. The transition between two power laws is evident in the slope change of the $log - log$ plot of Fig. S2.

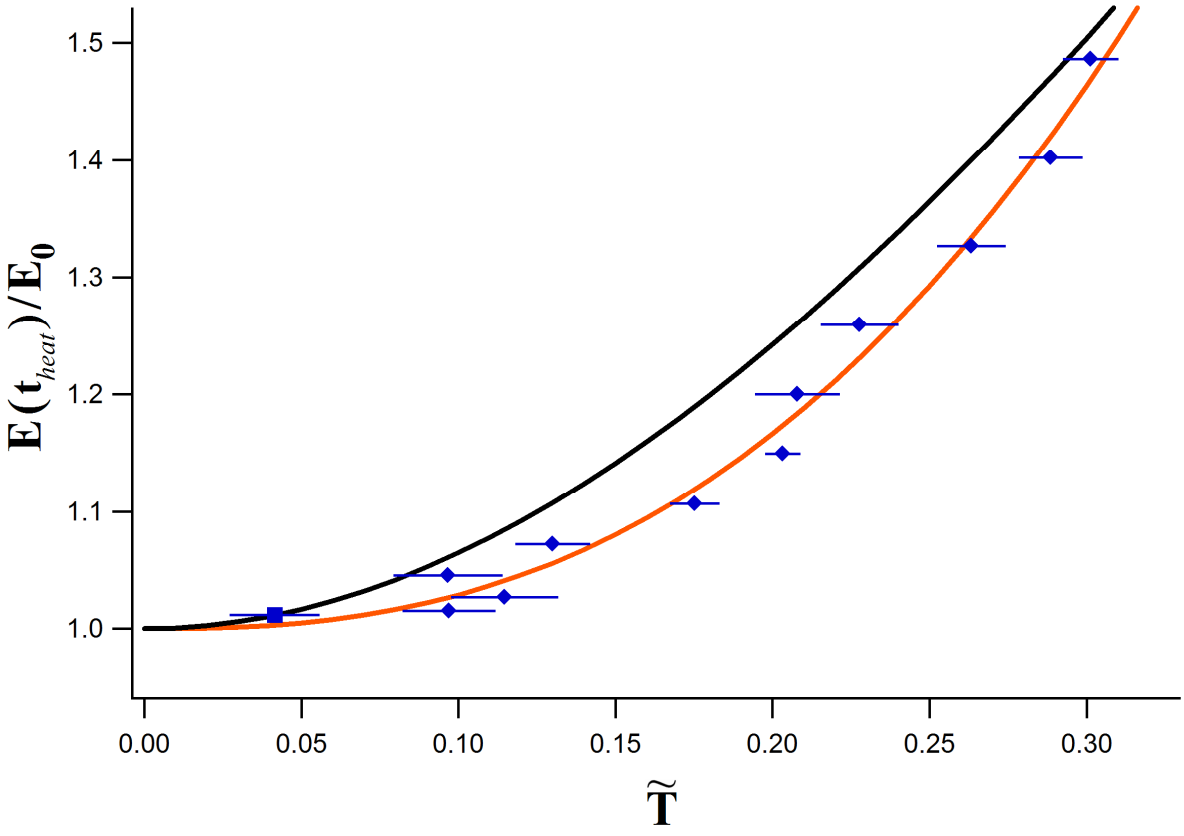

Figure S1: Strongly-interacting Fermi gas below the transition temperature. E/E_0 versus uncalibrated empirical temperature $\tilde{T}$ on a linear scale. Orange line, best fit power law $9.8\,\tilde{T}^{2.53}$. Black curve: Predicted E/E_0 for an ideal Fermi gas as a function of $\tilde{T} = T/T_F$. Note the lowest temperature point (blue square) is not included in the fits: It is constrained to lie on the black curve by our choice of $\eta_{int} = 1.01$ in Eq. 2 of the main text.

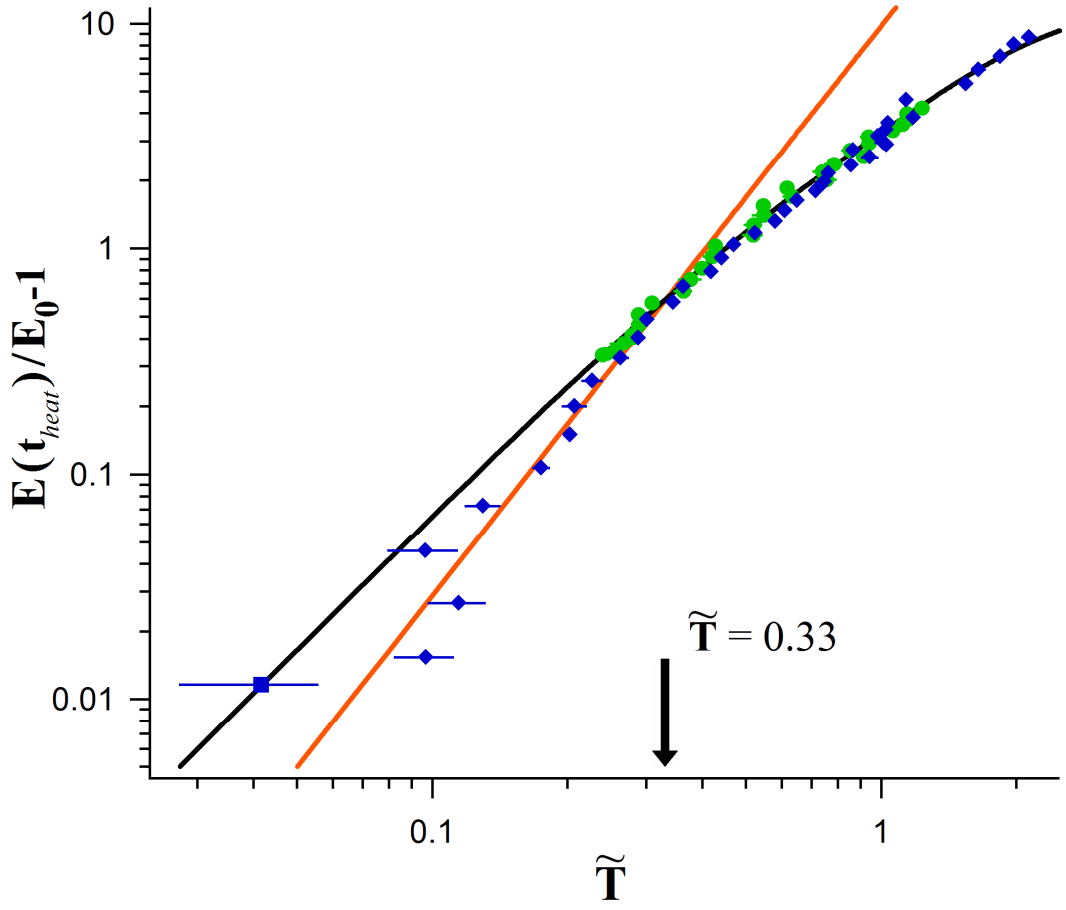

Figure S2: Energy input versus uncalibrated temperature $\tilde{T}$ on a $log-log$ scale. The strongly interacting Fermi gas shows a transition in behavior near $\tilde{T} = 0.33$. Green circles: noninteracting Fermi gas data; Blue diamonds: strongly interacting Fermi gas data. Black curve, prediction for a noninteracting, trapped Fermi gas. Orange line, best fit power law $9.8\,\tilde{T}^{2.53}$. Note the lowest temperature point (blue square) is not included in the fits, as it is constrained to lie on the black curve.

References and Notes

S1. T.-L. Ho, *Phys. Rev. Lett.* **92**, 090402 (2004).

S2. A. Perali, P. Pieri, L. Pisani, G. C. Strinati, *Phys. Rev. Lett.* **92**, 220404 (2004).

S3. L. D. Carr, G. V. Shlyapnikov, Y. Castin, *Phys. Rev. Lett.* **92**, 150404 (2004).

S4. J. E. Williams, N. Nygaard, C. W. Clark, *New J. Phys.* **6**, 123 (2004).

S5. H. Heiselberg, *Phys. Rev. Lett.* **93**, 040402 (2004).

S6. H. Hu, A. Minguzzi, X.-J. Liu, M. P. Tosi, *Phys. Rev. Lett.* **93**, 190403 (2004).

S7. S. Stringari, *Europhys. Lett.* **65**, 749 (2004).

S8. J. Kinnunen, M. Rodriguez, P. Törmä, *Science* **305**, 1131 (2004).

S9. C. Chin (2004). ArXiv:cond-mat/0409489.

S10. K. M. O'Hara, *et al.*, *Science* **289**, 2179 (2002).

S11. Q. Chen, J. Stajic, S. Tan, K. Levin (2004). ArXiv:cond-mat/0404274.

S12. A. J. Leggett, *Modern Trends in the Theory of Condensed Matter* (Springer-Verlag, Berlin, 1980), pp. 13–27.

S13. J. Stajic, Q. J. Chen, K. Levin (2004). ArXiv:cond-mat/0402383.

S14. J. Stajic, *et al.*, *Phys. Rev. A* **69**, 063610 (2004).

S15. Q. Chen, J. Stajic, K. Levin (2004). ArXiv:cond-mat/0411090.

S16. A. Perali, P. Pieri, G. C. Strinati, *Phys. Rev. Lett.* **93**, 100404 (2004).

S17. J. Stajic, Q. Chen, K. Levin (2004). ArXiv:cond-mat/0408104.

S18. J. Maly, B. Jankó, K. Levin, *Physica C* **321**, 113 (1999).

S19. C. A. Regal, M. Greiner, D. S. Jin, *Phys. Rev. Lett.* **92**, 040403 (2004).

S20. M. Bartenstein, *et al.*, *Phys. Rev. Lett.* **92**, 120401 (2004).

S21. M. W. Zwierlein, *et al.*, *Phys. Rev. Lett.* **92**, 120403 (2004).

S22. J. Kinast, *et al.*, *Phys. Rev. Lett.* **92**, 150402 (2004).

S23. J. Kinast, A. Turlapov, J. E. Thomas, *Phys. Rev. A* **70**, 051401(R) (2004).

S24. K. M. O'Hara, S. L. Hemmer, M. E. Gehm, S. R. Granade, J. E. Thomas, *Science* **298**, 2179 (2002).

S25. C. Menotti, P. Pedri, S. Stringari, *Phys. Rev. Lett.* **89**, 250402 (2002).

S26. M. E. Gehm, S. L. Hemmer, S. R. Granade, K. M. O'Hara, J. E. Thomas, *Phys. Rev. A* **68**, 011401(R) (2003).

S27. J. Kinast, A. Turlapov, J. E. Thomas (2004). ArXiv:cond-mat/0409283.